Journal of Intelligent & Robotic Systems (2025) 111:82
https://doi.org/10.1007/s10846-025-02282-9

REGULAR PAPER

Localization Handover for Mobile Robots: A Seamless Indoor-Outdoor Approach

Yuan Cao[1] · Andrea Usai[1] · Weibin Gu[2] · Alessandro Rizzo[1]

Received: 19 December 2024 / Accepted: 9 June 2025

Abstract
This paper presents a seamless indoor-outdoor localization approach for autonomous mobile robots by integrating multiple technologies: Ultra-Wideband (UWB) for high-precision indoor positioning, Global Positioning System (GPS) for outdoor global navigation, odometry for detailed granularity, and an Inertial Measurement Unit (IMU) for responsive motion tracking. The method employs loosely coupled Extended Kalman Filters (EKFs) to fuse these data sources, dynamically adjusting based on signal quality to ensure continuous and reliable localization in transition areas. Through extensive validation in simulation environments, the proposed system demonstrates the ability to mitigate the challenges posed by incomplete localization coverage in indoor-outdoor transition zones. The results show significant improvement in localization accuracy, enabling safer and more efficient robot navigation across diverse environments. Quantitative comparisons with recent studies demonstrate that our method achieves localization performance similar to tightly-coupled approaches, yet with significantly lower computational complexity, simpler implementation, greater flexibility in sensor integration, and enhanced robustness to individual sensor failures.

Keywords Localization · Sensor fusion · Indoor-outdoor · Sensor handover · Kalman filter

1 Introduction

Modern robotic systems such as ground robots, autonomous vehicles and drones, has accelerated across various domains, including industrial automation, healthcare, education and domestic applications. As these systems grow more sophisticated, ensuring reliable and precise localization becomes essential to safety, efficiency, and robust navigation [1]. Despite significant advances in sensor and computing technologies, localization remains a multifaceted challenge due to varying environmental conditions and the specific requirements of each application.

In the last decade, numerous localization techniques have been developed for both indoor and outdoor environments. In outdoor scenarios, Global Navigation Satellite System (GNSS) is widely considered one of the most reliable technologies for global positioning. However, it faces significant limitations in urban canyons, where Non-Line-Of-Sight (NLOS) conditions and multipath propagation degrade performance [2]. These challenges are even more severe in complex indoor environments, where GNSS signals are often obstructed or entirely unavailable. To meet the pressing demands for indoor localization, various specialized techniques such as Received Signal Strength Indicator (RSSI), UWB and Simultaneous Localization and Mapping (SLAM) have been developed. Although each approach has shown promise, they also exhibit inherent drawbacks. For instance, RSSI-based systems offer a simple and cost-effective solution by estimating the distance between a transmitter and receiver based on signal strength and using a nonlinear model. However, they struggle with reduced accuracy and are highly susceptible to noise, particularly in complex indoor environments due to the multipath fading problem [3]. On the other hand, UWB technology provides high-precision

✉ Alessandro Rizzo
alessandro.rizzo@polito.it

Yuan Cao
yuan.cao@polito.it

Andrea Usai
andrea.usai@polito.it

Weibin Gu
guweibin@air.tsinghua.edu.cn

[1] Department of Electronics and Telecommunications, Politecnico di Torino, Corso Duca degli Abruzzi, 24, 10129 Torino, Italy

[2] Institute for AI Industry Research (AIR), Tsinghua University, Beijing 100084, PR China

Published online: 24 July 2025

indoor positioning by leveraging wide bandwidth and effective multipath interference mitigation. Nevertheless, it incurs high costs and limited range, especially in NLOS environments [4]. Lastly, SLAM techniques, primarily based on the use of stereo camera or LiDAR sensors, enable the robot to map unknown environments while simultaneously determining its own position but they suffer from error accumulation and significant computational demands [5].

As a result, reliance on any single method fails to ensure the performance one would expect from autonomous systems, especially across diverse environments [6, 7]. Indeed, these standard approaches make the achievement of a *seamless Indoor-Outdoor (IO) localization* particularly difficult in applications such as warehouse automation or smart homes, which require continuous and smooth operations of autonomous robots across both IO settings [8, 9]. In transitional zones, where no single localization method attains its ideal accuracy, the development of robust, integrated localization strategies is crucial to maintain both safety and operational efficiency of autonomous systems. When partial signal loss occurs, robots should be able to dynamically adjust localization sources according to the environmental changes, thereby preserving localization accuracy and reliability.

To tackle this problem, we introduce the concept of *localization handover*, which refers to the seamless transition between distinct localization signals or methods—such as those optimized for indoor and outdoor settings—to guarantee uninterrupted and accurate positioning for mobile robots. By dynamically evaluating signal quality, environmental context, and accuracy requirements, localization handover helps prevent disruptions and maintain robust navigation. Realizing this concept involves two main challenges: (i) mitigating abrupt signal transitions that can result in inaccuracies, and (ii) identifying optimal switching conditions to balance reliability and computational efficiency.

A promising avenue to address these challenges lies in sensor fusion. By merging signals from multiple localization systems—including GNSS, UWB, and other sensor modalities—transitional zones can be bridged more effectively [10, 11]. Fusing multiple signals helps mitigate each system's weaknesses: for instance, leveraging GNSS for global reference in open spaces, UWB for accurate ranging indoors, and relative sensors like odometry and IMU for high-frequency data. Various fusion algorithms, such as EKF [12], Unscented Kalman Filter (UKF) [13], and Particle Filtering (PF) [14], can be employed to combine these signals. Among these, the EKF often provides a favorable balance between accuracy, robustness, and computational demands, making it well-suited for embedded mobile robotic platforms [15].

Building on these insights, this work introduces a novel approach to the localization handover problem for mobile robots navigating mixed IO environments. In particular, we adopt an EKF-based loosely coupled sensor fusion framework that synthesizes signals from UWB, GPS, odometry, and IMU, thereby ensuring consistent and accurate localization indoors, outdoors, and during transitions. Our method dynamically adjusts fusion rates to reflect varying signal qualities in real-time, thus enhancing positioning reliability. By effectively integrating multiple localization technologies and enabling adaptive behavior in transitional regions, the proposed framework delivers a robust solution that meets the needs of autonomous systems in increasingly complex and dynamic environments. The remainder of this paper is organized as follows: Section 2 reviews existing research on localization technologies and seamless IO localization, examining various approaches and their limitations. Section 3 provides a detailed description of the technical framework underlying our proposed approach. Section 4 presents the simulation validation conducted to assess the effectiveness of our method. Finally, Section 5 offers concluding remarks and discusses potential avenues for future work.

2 Related Work

2.1 Sensor Fusion for Enhanced Localization

Several studies have focused on the integration of various localization systems using different types of sensor fusion techniques to achieve precise localization. An in-depth examination [16] presents the use of an EKF alongside map matching to significantly enhance navigation and tracking accuracy in low-cost land vehicles in outdoor areas. This approach effectively mitigates some of the limitations of standalone GPS or Inertial Navigation System (INS) systems by using their complementary strengths. Another study [17] utilizes an UKF to merge data from accelerometers, gyroscopes, and encoders for precise mobile robot localization. This method effectively combines two dead reckoning techniques, reducing errors associated with single-method approaches. However, cumulative positioning errors over time limit its suitability for long-term localization. Further research [18] and [19] demonstrates the use of PF to fuse data from GNSS, inertial sensors (such as MEMS-IMU) and other sensors in applications of augmented reality and RPAS navigation in outdoor areas. These methods significantly improve tracking and navigation accuracy and stability, although with increased computational demands. Similarly, it is confirmed in [15] that for mobile robot localization, PF surpasses EKF in state estimation accuracy for nonlinear, non-Gaussian systems, though at a higher computational cost. To improve indoor positioning, a federated derivative Cubature Kalman Filter (CKF) [20] was developed, combining IMU and UWB data. This approach optimizes computational efficiency and accuracy while using Singular Value Decomposition (SVD) to improve convergence stability.

Previous studies adopted sensor fusion techniques to enhance localization accuracy in individual scenarios. In contrast, our proposed method targets seamless localization between indoor and outdoor areas. The achievement of seamless integration depends on the effective integration of indoor localization technologies with outdoor systems like GNSS. Several studies have explored how different indoor positioning technologies can be harmoniously integrated with GNSS, paving the way for a smooth and seamless navigation experience in diverse environments (see Table 1 for a summary of existing methods).

2.2 Localization Handover in IO environments

In [21], a system integrating INS, GNSS, and LiDAR was developed to facilitate seamless navigation. The proposed approach employs GNSS/INS for outdoor localization and INS/LiDAR for indoor navigation, with modality switching determined by evaluating the Horizontal Dilution of Precision (HDOP) value to assess GPS signal quality. Another approach presented in [22] integrates GNSS/INS for outdoor and Wi-Fi/INS for indoor navigation, using an EKF for data fusion, with the transition between navigation modes guided by GNSS signal quality metrics like Signal-to-Noise Ratio (SNR) or Carrier-to-Noise Density (C/N0). Further work in [23] combines GNSS and INS for outdoor navigation and pairs INS with *Locata,* a terrestrial ranging technology for indoor positioning, using a Federated Kalman Filter (FKF) to fuse data from these systems. Furthermore, [24] proposed a prototype for seamless IO infrastructure-free positioning of pedestrians and vehicles, which uses GNSS-aided foot-mounted IMU for outdoor localization, while relying on

Table 1 Summary of existing methods for seamless indoor-outdoor localization

Ref	Year	Platform	Indoor	Outdoor	Handover Approach
[36]	2008	Customized[1]	WSN	GNSS	Signal quality assessment
[35]	2009	Smartphone	Wi-Fi	GNSS	Loosely coupled (EKF); SNR-based switching
[37]	2013	Smartphone	Wi-Fi/MARG	GNSS	Loosely coupled (EKF)
[22]	2014	Customized[2]	Wi-Fi/INS	GNSS/INS	EKF-based integration; SNR switching
[38]	2016	Smartphone	Wi-Fi	GNSS	Context-based handover
[23]	2017	Customized[3]	Locata/INS	GNSS/INS	FKF-based integration
[2]	2017	Mobile Robot	Terrestrial ranging/INS	GNSS/INS	Loosely coupled (FKF)
[34]	2018	Smartphone	INS/MARG	GNSS	Loosely coupled (PF)
[39]	2019	Vehicle	Visual odometry/Camera	GNSS/INS	Integrated w/ visual odometry
[24]	2019	Wearable Device	IMU	GNSS	Loosely coupled, triggers on GNSS accuracy indicators
[31]	2019	Mobile Robot	UWB	GNSS	Loosely coupled, weighted fusion algorithm
[21]	2020	Mobile Robot	INS/LiDAR	GNSS/INS	Handover via HDOP
[40]	2021	Autonomous Vehicle	LiDAR	GNSS	Loosely coupled, HDOP-based transitions
[29]	2021	Mobile Robot	UWB	GNSS/INS	Tightly coupled (EKF), uses PPP/RTK
[41]	2023	Mobile Robot	UWB	GNSS	Tightly coupled (Federated Filter)
[30]	2023	UGV	UWB	GNSS/INS	Tightly coupled, two-step weighting model
[28]	2023	UGV	UWB/INS	GNSS/INS	Hybrid (ES-KF), dynamic fusion in transition
[32]	2023	Vehicle	UWB	GNSS	Loosely coupled w/ Ceres optimization

[1] A custom semi-physical simulation platform
[2] A custom hardware-based low-cost pedestrian navigation system
[3] A custom hardware-based GNSS/INS/Locata integrated navigation system

IMU data for indoor localization. A loosely coupled system facilitates seamless localization by utilizing a horizontal position accuracy indicator from the GNSS receiver to detect transitions and enable handover. However, LiDAR provides accurate 3D mapping and object recognition capabilities, but is constrained by its high cost, sensitivity to environmental factors such as dust and smoke, and the need for significant computational resources [25]. WLAN technology has drawbacks such as susceptibility to signal interference, multipath propagation in which signals bounce off surfaces causing errors, variability in signal strength due to environmental changes or device density, and poor positioning accuracy [26]. Pseudolite technology, like Locata, faces challenges such as interference and multipath effects [27]. The high deployment and maintenance costs are also their significant drawbacks.

In response to these challenges, UWB has become a popular choice for indoor localization due to its high accuracy, robustness against multipath interference, and fine time resolution. In [28], a system using UWB, GNSS, INS, and an (ES-KF) was developed for seamless IO positioning. This method employs tightly coupled UWB and INS for indoor positioning and loosely coupled GNSS and INS for outdoor positioning. In transitional areas, it dynamically fuses preprocessed UWB ranging measurement with GNSS position information. Similarly, the study presented in [29] introduces a tightly integrated system combining GNSS, INS, and UWB. To further increase accuracy, it uses Precise Point Positioning (PPP) and Real Time Kinematic (RTK) with INS for outdoor positioning. In transitional areas, it incorporates carrier phase measurements as GPS distance measurements alongside UWB ranging measurements to refine positioning, even when signals are partially blocked. In [30], a tightly coupled PPP/INS/UWB positioning system was introduced. In contrast to previous studies, this approach relies solely on UWB for indoor localization, supplemented by an alternative processing step. It dynamically determines the environment based on the geometric distribution of UWB anchors and employs a two-step weighting model to enhance UWB localization accuracy. Another framework, presented in [31], employs an adaptive approach to fuse data from GPS, UWB, and Magnetic, Angular Rate, and Gravity (MARG). This system also relies on UWB for indoor localization and uses a weighted fusion algorithm to integrate positioning data from different sources in transitional zones. Lastly, [32] integrated GPS with UWB using the *Ceres* [33] optimization framework, a nonlinear least-squares solver, to achieve seamless and accurate localization in transitional zones.

While these studies have shown promising results for IO localization by integrating various sensors and employing different fusion techniques, methods like ES-KF [28] and the nonlinear optimization algorithm in *Ceres* [32] demand high computational loads and are resource-intensive. In addition, tightly coupled approaches [28–30], which jointly processing raw data from multiple sensors, make overall performance highly sensitive to individual measurements—errors or failures in a single sensor can significantly affect the entire system. For instance, the approach in [29] applies a unified EKF to jointly process raw GNSS pseudorange, single-anchor UWB range measurements, and IMU data. By coupling all these raw observations at the same estimation level, it can achieve higher accuracy when each sensor is functioning properly. However, if the single-anchor UWB measurement degrades or becomes unreliable (e.g., blocked line-of-sight or heavy multipath), the filter's overall performance deteriorates because it depends heavily on that one range reading for indoor positioning. Furthermore, this architecture complicates expansion or modification: adding multiple UWB anchors or switching to a different ranging technology typically requires substantial reconfiguration of the core filter. Consequently, the lack of modularity and scalability makes it challenging to adapt to new sensors or dynamic conditions, as altering one component often necessitates an extensive recalibration or redesign of the entire system. Weighted fusion algorithms [31] relying solely on certain quantifiable metrics of the current signal for weight assignment lack dynamic state prediction and feedback mechanisms, making them unable to effectively handle nonlinear system errors or adapt to dynamic environmental changes. The lack of historical data utilization prevents effective state smoothing, which may lead to abrupt jumps in positioning results. Moreover, methods [30–32] relying solely on UWB for indoor positioning may face robustness issues in challenging environments. Li et al. [30] is highly dependent on pre-planned area recognition and precise anchor placement, limiting their adaptability in dynamic or unknown environments. Furthermore, other loosely coupled methods [31, 32] lack predictive mechanisms and do not incorporate historical information for smoothing transitions. Meanwhile, approaches such as [24, 34, 35] focus narrowly on signal-quality-based switching without integrating motion models or hierarchical estimation structures.

Our approach addresses these limitations by leveraging the EKF in a loosely coupled manner to dynamically fuse data from GPS, UWB, IMU, and odometry based on signal quality. By incorporating two relative localization data sources (IMU, Odometry) as the foundation for fusion, our method enhances robustness against individual sensor failures and reduces computational load by avoiding the joint processing of raw sensor data. The loosely coupled architecture provides

modularity and scalability, allowing for easy adaptation to new sensors or changing conditions without necessitating extensive system redesign. Additionally, EKF offers dynamic state prediction, enabling our method to handle nonlinear errors and adapt to changing environments. By utilizing historical data, we achieve smooth positioning results without abrupt jumps. This provides a more efficient, robust, and adaptable system for seamless IO localization, effectively overcoming the shortcomings of existing methods and filling the gaps in current research.

3 Methodology

In this section, we begin by presenting the technical background, which includes the kinematics model of the differential drive robot—an essential component for formulating the system dynamics within the EKF—and a detailed description of the sensor configuration used for localization. We then proceed to elaborate our localization handover strategy, including fusion approach across indoor and outdoor environments and the algorithmic workflow. The latter part of this section is devoted to the implementation details, explaining how both the local and global EKFs operate individually and collectively to ensure seamless and robust localization across varying environmental conditions.

3.1 Technical Background

3.1.1 Differential Drive Robot Kinematics

Here, we consider a differential drive robot moving on a planar surface. The robot's motion is described by its wheel velocities, with two wheels positioned on either side of the robot. To describe its kinematics, we define three reference frames: (i) inertial frame (X_I, Y_I, Z_I), (ii) odometry frame (X_O, Y_O, Z_O), and (iii) body frame (X_B, Y_B, Z_B), as shown in Fig. 1. The inertial frame serves as the global reference system, providing a coordinate framework essential for absolute positioning and orientation, particularly when integrating data from global sensors such as GPS and UWB. It is typically aligned with the East-North-Up (ENU) coordinate system, where the X_I axis points east, the Y_I axis points north, and the Z_I axis points upward. The odometry frame is defined on the basis of the robot's initial position and orientation at the start of motion. It remains fixed with respect to the inertial frame and serves as an intermediate frame to accumulate the relative motion estimated from odometry and IMU

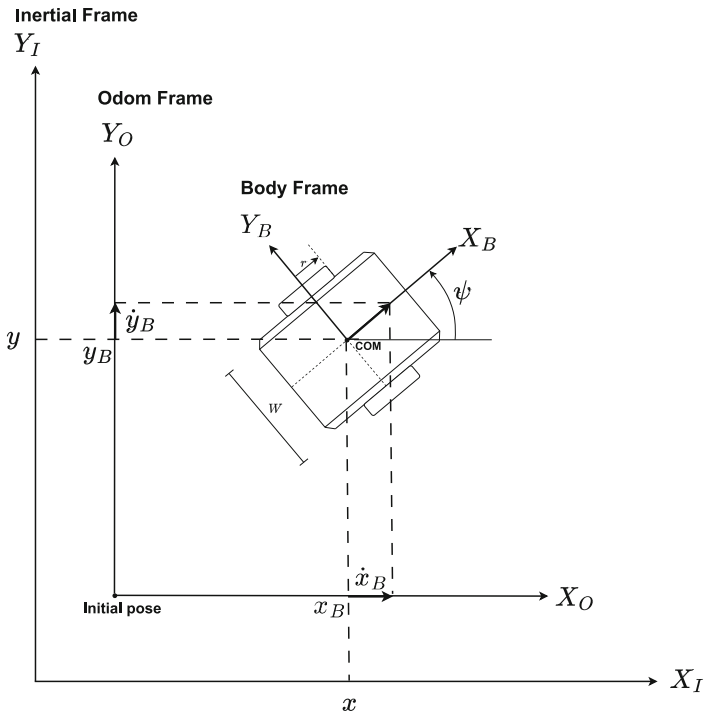

Fig. 1 Free body kinematics for differential drive robot

measurements. The body frame is fixed to the robot itself, aligning with its physical structure, and is used to express sensor measurements and control commands relative to the robot's Center Of Mass (COM) and moves with the robot. Its X_B axis points forward along the robot's heading, the Y_B axis points to the left side of the robot, and the Z_B axis points upward, perpendicular to the plane of motion. To facilitate the conversion between these frames, we define the following Transformation Matrices (TFs), each represented as a 4×4 homogeneous TF within the group of Special Euclidean transformations, denoted as $SE(3)$:

- $\mathbf{TF_{O\to I}} \in SE(3)$: This TF represents the transformation from the odometry frame to the inertial frame. It includes both a rotation component $\mathbf{R} \in SO(3)$ and a translation vector $\mathbf{t} \in \mathbb{R}^3$, which align the global coordinate system to the robot's initial reference frame.
- $\mathbf{TF_{B\to O}} \in SE(3)$: This matrix represents the transformation from the body frame to the odometry frame. It tracks the robot's movement relative to its initial position and orientation using data from odometry and IMU sensors.
- $\mathbf{TF_{B\to I}} \in SE(3)$: This matrix represents the transformation from the body frame to the inertial frame, effectively combining the transformations $\mathbf{TF_{O\to I}}$ and $\mathbf{TF_{B\to O}}$ to provide a direct relationship between the global reference frame and the current pose of the robot.

Let $\mathbf{p} = [x, y, z]^\top \in \mathbb{R}^3$ denote the position of the robot's COM in the inertial frame. Assuming a planar motion, let $\mathbf{v} = [\dot{x}_B, \dot{y}_B, 0]^\top \in \mathbb{R}^3$ represent the linear velocity of the body frame relative to the odometry frame, with $\dot{z}_B = 0$. The angular velocity, defined as $\boldsymbol{\omega} = [0, 0, \dot{\psi}]^\top \in \mathbb{R}^3$, captures the yaw rate $\dot{\psi}$, where ψ specifies the orientation of the body frame relative to the odometry frame. The inertial velocities $\dot{x}$ and $\dot{y}$ are thus derived from the local body-frame velocities $\dot{x}_B$ and $\dot{y}_B$ as follows:

$$\begin{bmatrix}\dot{x}\\ \dot{y}\end{bmatrix} = \begin{bmatrix}\cos\psi & -\sin\psi\\ \sin\psi & \cos\psi\end{bmatrix}\begin{bmatrix}\dot{x}_B\\ \dot{y}_B\end{bmatrix}. \tag{1}$$

3.1.2 Sensor Configuration

The proposed localization system utilizes data from various sensors as input for two EKFs. These consist of the Local EKF for relative localization and the Global EKF for absolute localization, with sensors integrated into this framework as follows:

GPS provides absolute position measurements when operating in outdoor environments. The GPS receiver outputs raw data in the form of Latitude, Longitude, and Altitude (LLA) coordinates in the world geodetic system. To integrate these measurements into our localization framework, we converted the LLA coordinates to the inertial coordinate frame using the Navsat node. The Navsat node [42] transforms the geodetic coordinates into local Cartesian coordinates relative to a defined reference point, resulting in position data $\mathbf{p} = [x, y, z]^\top$ in the inertial frame. This conversion is essential for aligning the GPS data with other sensor measurements within the same coordinate system. Additionally, the GPS receiver provides the HDOP, which indicates the quality of the satellite geometry and affects the measurement covariance. These absolute position measurements in the inertial frame are crucial for global localization and are used to update the robot's position in the global EKF.

UWB offers absolute position measurements in indoor environments where GPS signals are not available or degraded. The UWB system comprises anchors placed at known positions and a mobile tag on the robot, providing range measurements used to compute the robot's position through trilateration. The output is the robot's position $\mathbf{p} = [x, y, z]^\top$ in the inertial frame. These measurements serve as the main source of absolute indoor positioning and are integrated into the global EKF.

IMU supplies high-frequency measurements of angular velocities $\boldsymbol{\omega} = [\dot{\phi}, \dot{\theta}, \dot{\psi}]^\top$ and linear accelerations $\mathbf{a} = [\ddot{x}_B, \ddot{y}_B, \ddot{z}_B]^\top$ in the robot's odometry frame. By integrating these measurements, the IMU provides estimates of the robot's orientation angles $\boldsymbol{\theta} = [\phi, \theta, \psi]^\top$ and contributes to the estimation of the robot's linear velocities $\mathbf{v} = [\dot{x}, \dot{y}, \dot{z}]^\top$ and relative position changes. The IMU data are essential for estimating the dynamic motions and orientation of the robot, and are utilized in both the local and global EKFs.

Odometry utilizes wheel encoders to measure the rotations of the left and right wheels, providing raw angular velocity data ω_{left} and ω_{right}, yielding

$$\dot{x}_B = \frac{r}{2}(\omega_{\text{left}} + \omega_{\text{right}}), \tag{2}$$

$$\dot{\psi} = \frac{r}{W}(\omega_{\text{right}} - \omega_{\text{left}}), \tag{3}$$

where r is the radius of the wheels. These velocities are crucial for estimating the robot's motion and are used directly in the local EKF for continuous state estimation. By integrating these velocities over time, odometry provides estimates of the robot's relative position changes, which are essential for short-term, relative localization, especially when absolute positioning data are unavailable. Using the differential drive kinematic model, these measurements are converted into the robot's linear velocities in the odometry frame $\dot{x}_B$, and its angular velocity $\dot{\psi}$. Specifically, linear velocities are

calculated based on the average of the left and right wheel speeds, while the angular velocity is derived from the difference between the wheel speeds divided by the wheelbase width W.

These sensors collectively provide the necessary data for the EKFs to estimate the robot's state, including position, velocity, and orientation. Table 2 summarizes the measurements from each sensor. For detailed principles and equations of the EKFs used in our methodology, please refer to Appendix A.

3.2 Localization Handover

In this section, we present our proposed fusion strategy for seamless IO localization, leveraging both Local and Global EKF. This hierarchical approach is based on a two-layer structure, where local state estimation runs continuously, and global corrections are applied asynchronously when available—reflecting a modular and loosely coupled design. In contrast to tightly coupled approaches, which directly fuse raw sensor measurements (e.g., GNSS pseudoranges, IMU accelerations, UWB ranges) within a single large-scale estimator, our method processes each sensor stream independently and fuses the resulting intermediate state estimates at a higher level. Tightly coupled architectures, although potentially offering slightly higher theoretical accuracy, require detailed sensor models and maintain high-dimensional state vectors. This leads to substantial computational burden due to the frequent manipulation of large covariance matrices, matrix inversions, and other intensive numerical operations at every update step. In comparison, our approach decomposes the estimation process into smaller, modular units, reducing the dimensionality of each sub-task and simplifying matrix computations. Moreover, by decoupling the global update from the fast-rate local estimation, it avoids unnecessary system-wide recalculations—significantly lowering overall computational complexity. This structure not only improves real-time efficiency on resource-constrained platforms but also enhances robustness by isolating sensor faults and provides greater flexibility for incorporating new or alternative sensors without reconfiguring the core estimation framework. This design ensures continuous and reliable localization across varying environmental conditions, including outdoor, indoor, and transitional areas.

Table 2 Sensor measurements used for EKF

Sensor	Reference Frame	Measured Data
GPS	Inertial frame	x, y, z
UWB	Inertial frame	x, y, z
IMU	Odometry frame	$\dot{\phi}_B, \dot{\theta}_B, \dot{\psi}_B, \ddot{x}_B, \ddot{y}_B, \ddot{z}_B$
Odometry	Odometry frame	$\dot{x}_B, \dot{\psi}_B$

3.2.1 Fusion Strategy across IO Environments

Our fusion strategy is designed to dynamically integrate sensor data based on the operational environment, ensuring robust localization across outdoor, indoor, and transitional zones. Central to this strategy are two EKFs, which work in tandem to balance high-frequency updates with periodic global corrections.

Outdoor Navigation

In outdoor environments, UWB signals are generally unreliable, resulting in high noise covariance. Consequently, localization relies primarily on GPS, IMU, and odometry data. The Global EKF prioritizes GPS measurements due to their absolute positioning capability, while the Local EKF maintains accurate relative positioning through IMU and odometry inputs.

Indoor Navigation

Indoors, GPS signals are significantly degraded, leading to high noise covariance. The system therefore depends on UWB for absolute localization, which is fused with IMU and odometry data. The Global EKF assigns higher weights to UWB measurements, leveraging their robustness to multipath effects and indoor interference, while the Local EKF continues to provide precise relative positioning.

Handover Navigation

During transitions between IO environments, both GPS and UWB data are intermittently available. The fusion strategy ensures robustness by dynamically adjusting the fusion ratio based on the current noise covariance of each sensor. The Global EKF integrates whichever absolute positioning data is available (GPS or UWB), while the Local EKF maintains relative localization. This dual-input approach mitigates potential errors from any single sensor source, ensuring continuous and accurate positioning.

3.2.2 Algorithm Workflow

Figure 2 illustrates the algorithm workflow, clarifying the integration of sensor data from GPS, UWB, IMU, and odometry. The localization algorithm operates within the inertial frame, the odometry frame, and the body frame. Three

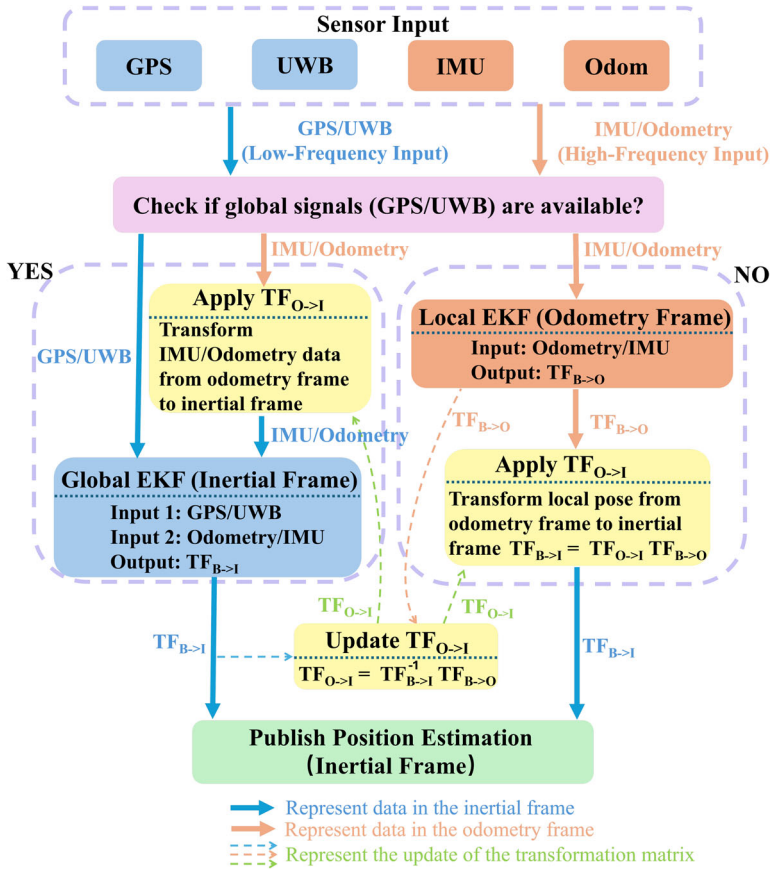

Fig. 2 Workflow for integration of Local and Global EKFs

transformation matrices (TFs) facilitate coherent integration of sensor data across these frames: odometry frame to inertial frame ($\mathbf{TF_{O\to I}}$), body frame to inertial frame ($\mathbf{TF_{B\to I}}$), and body frame to odometry frame ($\mathbf{TF_{B\to O}}$), as previously defined in Section 3.1.1.

Sensor Data Acquisition

The algorithm begins by acquiring inputs from GPS, UWB, odometry, and IMU sensors. GPS and UWB provide absolute localization directly in the inertial frame through $\mathbf{TF_{B\to I}}$. Conversely, odometry and IMU supply relative localization data initially in the odometry frame, captured via $\mathbf{TF_{B\to O}}$. These relative data are subsequently transformed into the inertial frame using the transformation matrix $\mathbf{TF_{O\to I}}$, initially set as an identity matrix when the odometry and inertial frames coincide at initialization. This ensures coherent representation of all sensor data within a unified coordinate system, facilitating seamless fusion with absolute positioning measurements.

Local EKF Processing

The Local EKF provides high-frequency, short-term relative positioning by integrating IMU and odometry measurements. In the prediction step, it predicts the local state estimate based on previous states. Subsequently, the update step corrects this predicted state with IMU and odometry measurements, updating $\mathbf{TF_{B\to O}}$ accordingly. When the Global EKF does not produce output (e.g., due to unavailability of GPS or UWB signals), the Local EKF uses $\mathbf{TF_{O\to I}}$ to transform the relative localization results from the odometry frame to the inertial frame, thereby obtaining global localization estimates.

Global EKF Processing

The Global EKF updates less frequently, specifically when new GPS or UWB data become available. It begins with a prediction step, estimating the global state from previous global state estimates. In the subsequent update step, it corrects this global state estimate using available absolute measurements (GPS or UWB) and relative measurements (IMU and

Algorithm 1 Localization Algorithm Using Local and Global EKFs

Initialization:
Initialize state estimates and covariance matrices for both EKFs.
Initialize $\mathbf{TF_{B\to O}}$, $\mathbf{TF_{B\to I}}$, $\mathbf{TF_{O\to I}}$
while Robot is operational **do**
  Acquire GPS, UWB, IMU, odometry data.

  Local EKF Processing:
  Prediction Step:
    Predict the local state estimate using the previous local state $\mathbf{x}_{\hat{L},k}$.
  Update Step:
    Correct the local state $\mathbf{x}_{L,k}$ and update $\mathbf{TF_{B\to O}}$ with IMU and odometry measurements.
  Coordinate Transformation:
    Compute the global position estimate:
      $\mathbf{TF_{B\to I}} \leftarrow \mathbf{TF_{O\to I}TF_{B\to O}}$.

  if New GPS or UWB data are available **then**
    Global EKF Processing:
    Prediction Step:
      Predict the global state estimate using the previous global state $\mathbf{x}_{\hat{G},k}$.
    Update Step:
      Correct the global state $\mathbf{x}_{G,k}$ and update $\mathbf{TF_{I\to B}}$ with GPS/UWB.
    Transformation Update:
      Update the transformation between inertial and odometry frames:
        $\mathbf{TF_{O\to I}} \leftarrow \mathbf{TF_{B\to I}TF_{B\to O}^{-1}}$.

  end if

  Output and Application:
  Provide the current global position estimate ($\mathbf{TF_{B\to I}}$) for navigation tasks.
end while

odometry) that are first transformed into the inertial frame via $\mathbf{TF_{O\to I}}$:

$$\mathbf{TF_{B\to I} = TF_{O\to I}TF_{B\to O}}, \tag{4}$$

This corrected global estimate then updates $\mathbf{TF_{B\to I}}$.

Transformation Update for Error Correction

When GPS or UWB data become available, the transformation $\mathbf{TF_{O\to I}}$ is recalibrated using:

$$\mathbf{TF_{O\to I} = TF_{B\to I}TF_{B\to O}^{-1}}, \tag{5}$$

This hierarchical fusion strategy effectively mitigates drift in relative localization without inducing abrupt shifts in the global coordinate system, thereby ensuring smooth and reliable state estimation across varying operational conditions. The localization procedure is summarized in the pseudocode of Algorithm 1.

3.2.3 Local EKF for Relative Localization

After outlining the overarching workflow of our localization algorithm, we now delve into the specific roles and implementations of the two essential components: the Local EKF for relative localization and the Global EKF for absolute localization. Understanding how these filters operate individually and in tandem is crucial for appreciating the robustness and accuracy of our hierarchical fusion strategy across varying environmental conditions.

The local EKF provides high-frequency, short-term localization by integrating measurements from the IMU and odometry sensors. It corrects for small errors and drifts between global updates.

State Vector

The state vector for the local EKF is:

$$\mathbf{x}_L = \left[x_B,\ y_B,\ z_B,\ \dot{x_B},\ \dot{y_B},\ \dot{z_B},\ \phi_B,\ \theta_B,\ \psi_B\right]^\top \in \mathbb{R}^9, \tag{6}$$

where (x_B, y_B, z_B) are the robot's coordinates, $(\dot{x_B}, \dot{y_B}, \dot{z_B})$ are the robot's linear velocities, and $(\phi_B, \theta_B, \psi_B)$ are the roll, pitch, and yaw angles representing the robot's orientation, all expressed in the odometry frame.

System Model

Using the kinematic equations, the state transition function in discrete time is

$$\mathbf{x}_{L,k+1} = \mathbf{x}_{L,k} + \mathbf{f}_L(\mathbf{x}_{L,k})\Delta t + \boldsymbol{\eta}_{L,k}, \tag{7}$$

where $\Delta t = t_{k+1} - t_k$ is the time step and $\boldsymbol{\eta}_{L,k}$ is the process noise with covariance matrix $\mathbf{Q}_{L,k}$. The function $\mathbf{f}_L : \mathbb{R}^9 \times \mathbb{R}^m \to \mathbb{R}^9$ is the nonlinear state transition model that captures the robot's motion dynamics, mapping the current state to the predicted state. In our implementation, $\mathbf{f}_L$ is defined as

$$\mathbf{f}_L(\mathbf{x}_{L,k}) = \left[\dot{x}_{B,k}\cos(\psi_{B,k}),\ \dot{x}_{B,k}\sin(\psi_{B,k}),\ 0,\ \ddot{x}_{B,k},\ \ddot{y}_{B,k},\ \ddot{z}_{B,k},\ \dot{\phi}_{B,k},\ \dot{\theta}_{B,k},\ \dot{\psi}_{B,k}\right]^\top, \tag{8}$$

so that the state transition function updates the position and orientation according to the robot's kinematics.

Measurement Model

The measurement vector is

$$\mathbf{z}_{L,k} = \left[\dot{x}^{\mathrm{m}}_{B,k}\ \ddot{x}^{\mathrm{m}}_{B,k}\ \ddot{y}^{\mathrm{m}}_{B,k}\ \ddot{z}^{\mathrm{m}}_{B,k}\ \dot{\phi}^{\mathrm{m}}_{B,k}\ \dot{\theta}^{\mathrm{m}}_{B,k}\ \dot{\psi}^{\mathrm{m}}_{B,k}\right]^\top + \boldsymbol{\nu}_{L,k}, \tag{9}$$

where $\dot{x}^{\mathrm{m}}_{B,k}$ is the linear velocity along the robot's forward direction, obtained from odometry; $\ddot{x}^{\mathrm{m}}_{B,k}, \ddot{y}^{\mathrm{m}}_{B,k}, \ddot{z}^{\mathrm{m}}_{B,k}$ are linear

accelerations from the IMU accelerometer; $\dot{\phi}^{\mathrm{m}}_{B,k}$ and $\dot{\theta}^{\mathrm{m}}_{B,k}$ are angular velocities around the roll and pitch axes, measured by the IMU gyroscope; $\dot{\psi}^{\mathrm{m}}_{B,k}$ is the angular velocity around the vertical axis derived from odometry and IMU—at time step k, $\boldsymbol{\nu}_{L,k}$ is the measurement noise with covariance matrix $\mathbf{R}_{L,k}$.

EKF Implementation

The local EKF operates according to a standard EKF framework, comprising two main steps:

Prediction Step

$$\hat{\mathbf{x}}_{L,k|k-1} = \hat{\mathbf{x}}_{L,k-1} + \mathbf{f}_L(\hat{\mathbf{x}}_{L,k-1})\Delta t, \tag{10}$$

$$\mathbf{P}_{L,k|k-1} = \mathbf{F}_{L,k-1}\mathbf{P}_{L,k-1}\mathbf{F}^{\top}_{L,k-1} + \mathbf{Q}_{L,k-1}. \tag{11}$$

Update Step

$$\mathbf{K}_{L,k} = \mathbf{P}_{L,k|k-1}\mathbf{H}^{\top}_{L,k}\left(\mathbf{H}_{L,k}\mathbf{P}_{L,k|k-1}\mathbf{H}^{\top}_{L,k} + \mathbf{R}_{L,k}\right)^{-1}, \tag{12}$$

$$\hat{\mathbf{x}}_{L,k} = \hat{\mathbf{x}}_{L,k|k-1} + \mathbf{K}_{L,k}\left(\mathbf{z}_{L,k} - \mathbf{h}_L(\hat{\mathbf{x}}_{L,k|k-1})\right), \tag{13}$$

$$\mathbf{P}_{L,k} = \left(\mathbf{I} - \mathbf{K}_{L,k}\mathbf{H}_{L,k}\right)\mathbf{P}_{L,k|k-1}. \tag{14}$$

For detailed definitions of $\mathbf{F}$, $\mathbf{P}$, $\mathbf{K}$, $\mathbf{H}$, $\mathbf{I}$ refer to Appendix A.

3.2.4 Global EKF for Absolute Localization

The global EKF corrects the accumulated errors in the local EKF by integrating the absolute position measurements from GPS and UWB.

State Vector

The global EKF uses the same state vector as the local EKF,

$$\mathbf{x}_G = \begin{bmatrix} x & y & z & \dot{x} & \dot{y} & \dot{z} & \phi & \theta & \psi \end{bmatrix}^{\top} \in \mathbb{R}^9. \tag{15}$$

System Model

The system model is similar to the local EKF:

$$\mathbf{x}_{G,k+1} = \mathbf{x}_{G,k} + \mathbf{f}_G(\mathbf{x}_{G,k})\Delta t + \boldsymbol{\eta}_{G,k}, \tag{16}$$

where $\boldsymbol{\eta}_{G,k}$ is the process noise with covariance $\mathbf{Q}_{G,k}$.

Measurement Model

The measurement vector for the global EKF includes absolute position measurements from GPS and UWB, as well as the state estimate from the Local EKF transformed into the inertial frame:

$$\mathbf{z}_{G,k} = \begin{bmatrix} x^{\mathrm{m}}_k \\ y^{\mathrm{m}}_k \\ z^{\mathrm{m}}_k \\ \mathbf{TF}_{\mathbf{O}\rightarrow\mathbf{I}}\,\mathbf{z}_{L,k} \end{bmatrix} + \boldsymbol{\nu}_{G,k}. \tag{17}$$

where: x_k, y_k, z_k are the absolute position measurements obtained from GPS and UWB sensors at time step k. $\mathbf{TF}_{\mathbf{O}\rightarrow\mathbf{I}}\mathbf{z}_{L,k}$ represents the state vector from the Local EKF ($\mathbf{z}_{L,k}$) transformed into the inertial frame using the $\mathbf{TF}_{\mathbf{O}\rightarrow\mathbf{I}}$. $\boldsymbol{\nu}_{G,k}$ is the measurement noise, assumed to be zero-mean Gaussian with covariance matrix $\mathbf{R}_{G,k}$.

The covariance for GPS measurements is computed using:

$$\sigma^2_{\mathrm{GPS}} = (\mathrm{HDOP} \times \sigma_{\mathrm{base}})^2, \tag{18}$$

where σ_{base} is the base standard deviation of the GPS receiver.

EKF Implementation

The global EKF uses the prediction and update steps as per the local EKF algorithm. However, it updates less frequently than the local EKF, i.e., only when new GPS or UWB data are available.

4 Results and Discussion

4.1 Simulation Environment

We defined an simulation scenario divided into indoor, outdoor, and transitional areas based on signal quality to validate our localization algorithm. As shown in Fig. 3(a), in the outdoor area A, the GPS signal coverage is complete, with a signal quality of 100%. Area B serves as a transitional zone where the signal gradually transitions from outdoor to indoor. Finally, area C is an indoor environment relying entirely on UWB for positioning. In our experiments, the robot starts its mission indoors and follows a predetermined reference path toward the outdoor environment, covering all areas to assess system performance under various signal conditions.

ROS2 Humble [43] was utilized to construct a simulation environment in Gazebo [44] as shown in Fig. 3(b), enabling us to test the algorithm performance in a controlled yet realistic setting. The TurtleBot3 Waffle robot [45] was employed for this purpose, with the "robot localization" package [46] supporting our experimental setup. In the simulation, we modeled the degradation of GPS and UWB signals by introducing varying levels of random noise, simulating the impact of different environments on localization accuracy. As the robot moves from outdoor to indoor environments, the GPS signal quality deteriorates, leading to increased noise. Conversely, UWB signal noise increases when transitioning from indoor to outdoor environments, reflecting an inverse relationship with GPS in terms of environmental impact on signal clarity. This setup allowed us to thoroughly assess the algorithm's robustness under varying conditions. In the simulation, we introduced gaussian white noise characterized by different variances to degrade the GPS and UWB

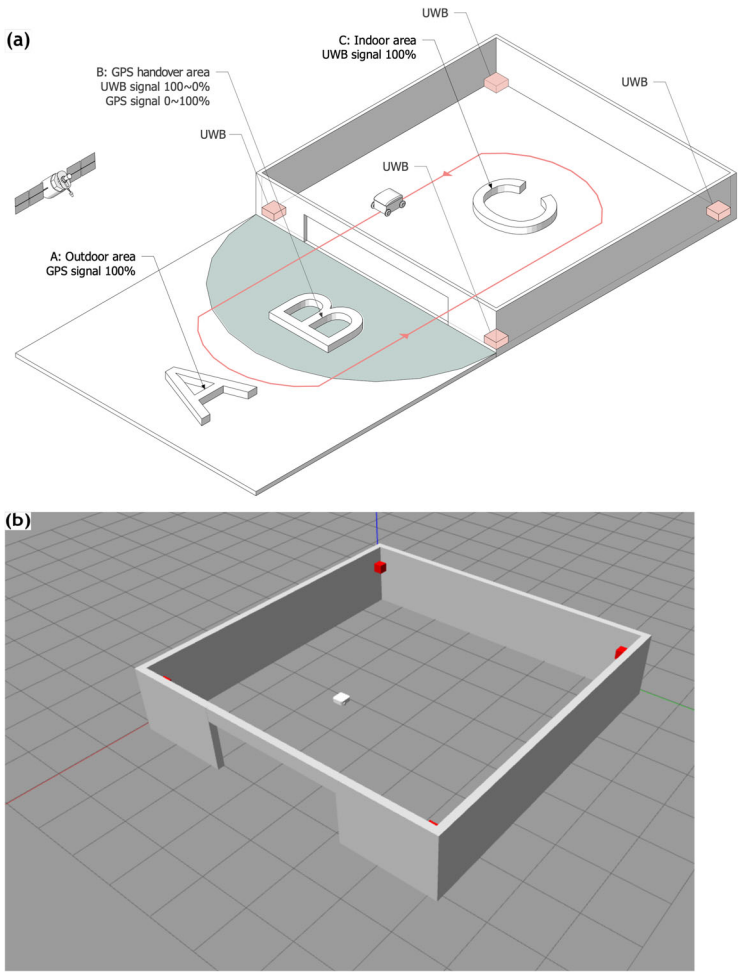

Fig. 3 Simulation setting. (a) The conceptual experimental environment. (b) The Gazebo simulation environment

signals under various environmental conditions. To better reflect realistic transitional behaviors, abrupt signal loss was avoided. Instead, signal degradation was modeled progressively by interpolating the noise variance based on the robot's position within the transition regions (e.g., doorways, corridor entries). The variance increases proportionally as the robot approaches the indoor (for GPS) or outdoor (for UWB) area, ensuring smooth transitions between sensor confidence levels and avoiding unrealistic signal drop-offs. Prior studies show that high-precision GNSS (e.g., GPS with PPP or RTK) can achieve accuracies of roughly 0.1–0.3 meters in open-sky environments, yet degrades to sub-meter or worse in urban canyons due to multipath effects and signal blockage [29]. Similarly, UWB accuracy is often below 0.2 m under ideal line-of-sight conditions, but can exceed 0.5–1 m in environments with significant multipath interference [47]. To capture this realistic range of performance, we selected three standard deviations—0.3, 0.6, and 0.9 m—for both GPS and UWB. These values represent mild, moderate, and more severe noise levels, respectively, enabling us to systematically evaluate our algorithm's robustness across different

Table 3 Noise levels for different areas (Unit: meters)

Area	GPS 1	UWB 1	GPS 2	UWB 2	GPS 3	UWB 3
Outdoor (A)	N/A	$\mathcal{N}(0, 0.3^2)$	N/A	$\mathcal{N}(0, 0.5^2)$	N/A	$\mathcal{N}(0, 0.7^2)$
Transitional (B)	$0 \sim \mathcal{N}(0, 0.3^2)$		$0 \sim \mathcal{N}(0, 0.5^2)$		$0 \sim \mathcal{N}(0, 0.7^2)$	
Indoor (C)	$\mathcal{N}(0, 0.3^2)$	N/A	$\mathcal{N}(0, 0.5^2)$	N/A	$\mathcal{N}(0, 0.7^2)$	N/A

$\mathcal{N}(\mu, \sigma^2)$ indicates Gaussian noise with mean μ and variance σ^2. $0 \sim \mathcal{N}(0, \sigma^2)$ indicates a transition from no noise to Gaussian noise with mean 0 and variance σ^2

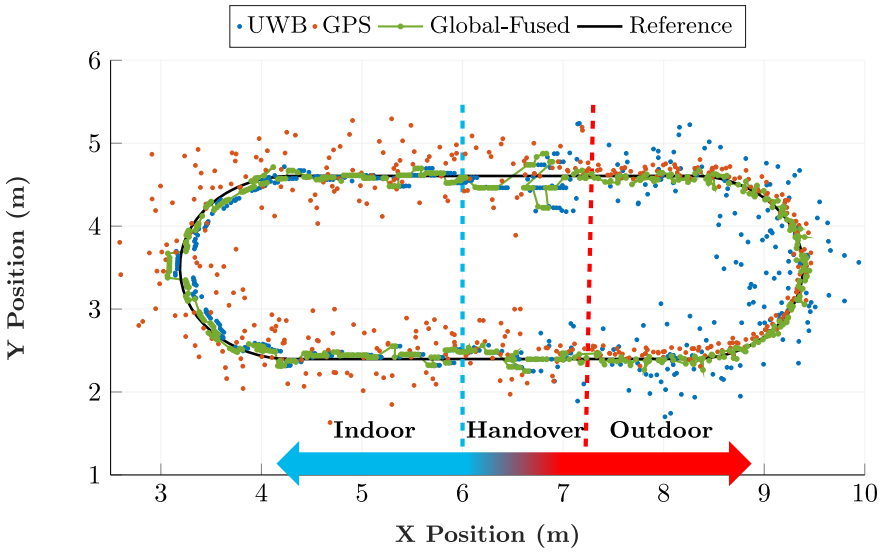

Fig. 4 Comparison of UWB, GPS, and Global-Fused localization result for path O with $\mathcal{N}(0, 0.3^2)$, showing alignment with the reference trajectory

sensor-accuracy scenarios. Table 3 summarizes the specific noise configurations applied in each region.

In addition, two routes were designed to verify the seamless handover between different areas while maintaining localization accuracy. The first route is shaped like the circular track of a classic stadium, as shown in Fig. 4, which we simply refer to as the shape "O". The second route goes back and forth between IO areas, as shown in Fig. 5, which we simplify as shaped as a "S". Both routes start from an indoor setting, pass through the gray handover area to the outdoors, and finally return to the indoors. This approach verifies that the algorithm can maintain high handover accuracy during transitions from indoor to outdoor and vice versa.

4.2 Simulation Results

The coordinate comparison of the localization signals is presented in Figs. 4 and 5. These figures depict the positioning data along path O and path S, demonstrating a comparison between different localization techniques under a noise condition with a standard deviation of 0.3. The main components of the plot include UWB localization positions, GPS localization positions, and the global-fused localization positions, all compared against the reference path. The UWB signal shows significant scatter in outdoor regions, indicating lower accuracy where the coverage is limited, while it is more reliable indoors due to anchor placement. Conversely, the GPS signal

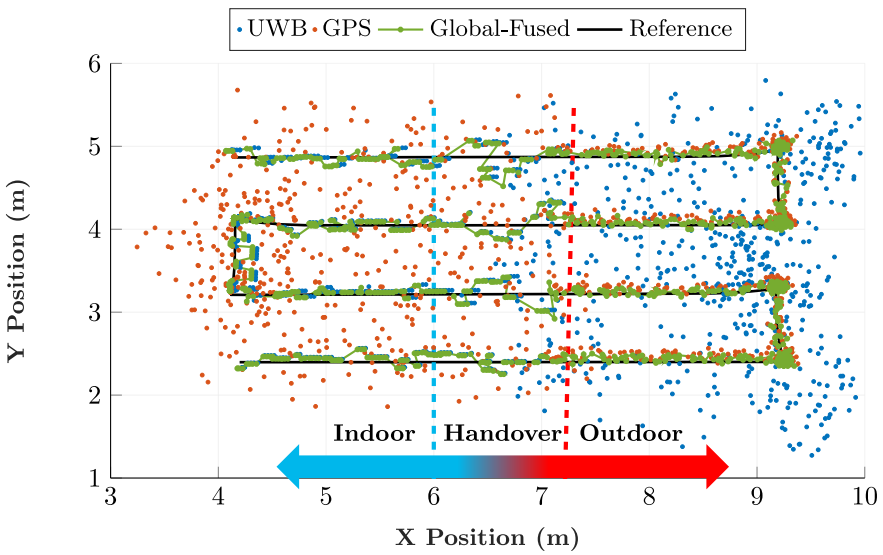

Fig. 5 Comparison of UWB, GPS, and Global-Fused localization result for path S with $\mathcal{N}(0, 0.3^2)$, showing alignment with the reference trajectory

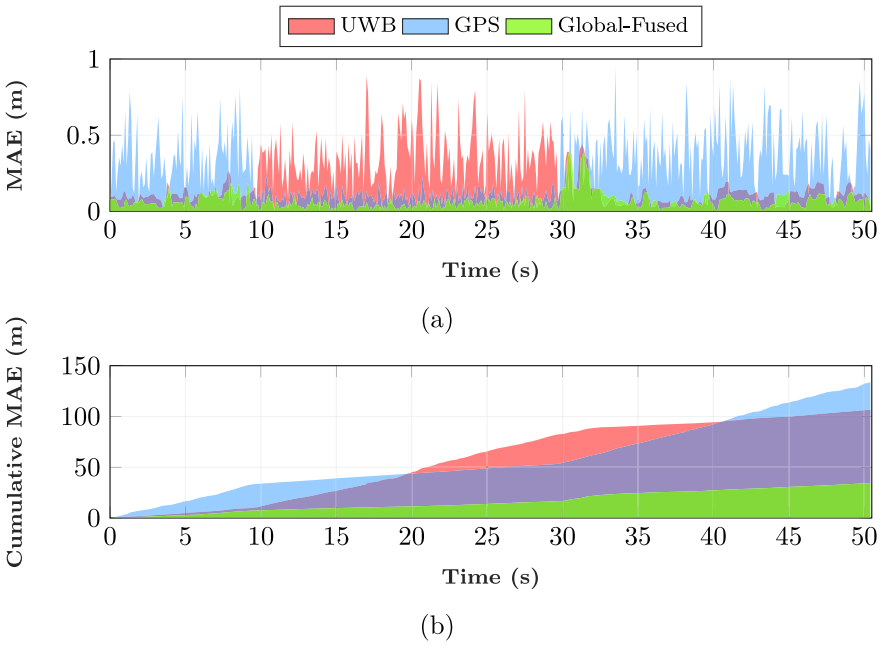

Fig. 6 Mean Absolute Error (MAE) of path O with $\mathcal{N}(0, 0.3^2)$. (a) Mean Absolute Error (MAE) variation over time. (b) Cumulative MAE over time

performs better outdoors but is less accurate indoors, where satellite signals are obstructed. The global fused trajectory closely follows the reference path, effectively blending UWB and GPS strengths: it relies more on UWB for indoor positioning and GPS for outdoor positioning. In the handover area, where neither GPS nor UWB is fully available, the fusion algorithm faces increased error compared to purely indoor or outdoor regions. Despite this, the error in the fused solution is still smaller than that of either individual signal, demonstrating that the fusion method continues to offer a more accurate estimate even under challenging conditions.

Figures 6 and 7 present the MAE analysis for path O and path S, comparing UWB, GPS, and global-fused localization methods over time under $\mathcal{N}(0, 0.3^2)$. Figures 6(a) and 7(a) shows the real-time MAE, where UWB and GPS have significant errors and fluctuations, particularly due to their respective limitations in outdoor and indoor environments. The global-fused method shows consistently lower errors,

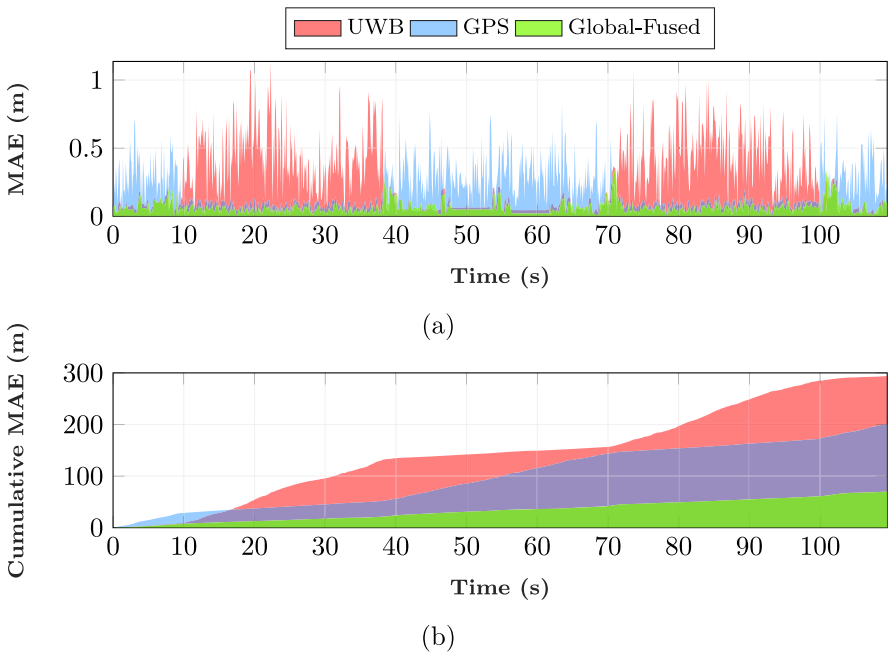

Fig. 7 Mean Absolute Error (MAE) of path S with $\mathcal{N}(0, 0.3^2)$. (a) MAE variation over time. (b) Cumulative MAE over time

demonstrating better accuracy by leveraging the strengths of both signals. In particular, when the red and blue regions alternate, it indicates a handover between the two signals. During these handover periods, the MAE of the global-fused method shows a noticeable increase, reflecting the challenges in maintaining accuracy when neither signal is fully reliable. Figures 6(b) and 7(b) illustrate the cumulative MAE, where the global fused approach accumulates the least error over time, outperforming both UWB and GPS.

Figures 8 and 9 present the Monte Carlo simulation results for the O and S path under varying noise levels. Each noise level was evaluated using 20 different random seeds, with the resulting trajectories demonstrating consistent behavior between trials, which emphasizes the reliability and robustness of the algorithm under different noise conditions. MSE tends to increase as the noise level increases, indicating the challenges in maintaining localization accuracy in environments characterized by greater uncertainty. The two notable peaks of MSE in path O observed at approximately 8s, 30s and the four notable peaks in path S observed at approximately 8s, 38s, 70s, and 105s coincide with periods of signal handover, due to the inherent difficulty in accurately estimating position when neither signal is fully reliable.

The overall mean and standard deviation of the MSE for each noise level and path are summarized in Table 4. It is evident that as the noise level increases, the overall mean MSE also tends to increase, reflecting the challenges in maintaining the accuracy of the localization under greater uncertainty. Despite this trend, the global-fused approach continues to demonstrate resilience by maintaining a relatively low standard deviation, indicating consistent performance across multiple trials.

Additionally, to further quantitatively assess the performance of the proposed method, we compare our approach with existing tightly-coupled GNSS/INS/UWB integration methods from previous studies. Li et al. [30] reported their results using Root Mean Square Error (RMSE) separately for east (0.339 m) and north (0.291 m) directions. To facilitate a direct comparison with our reported MSE, we calculated the two-dimensional horizontal MSE (ignoring vertical errors)

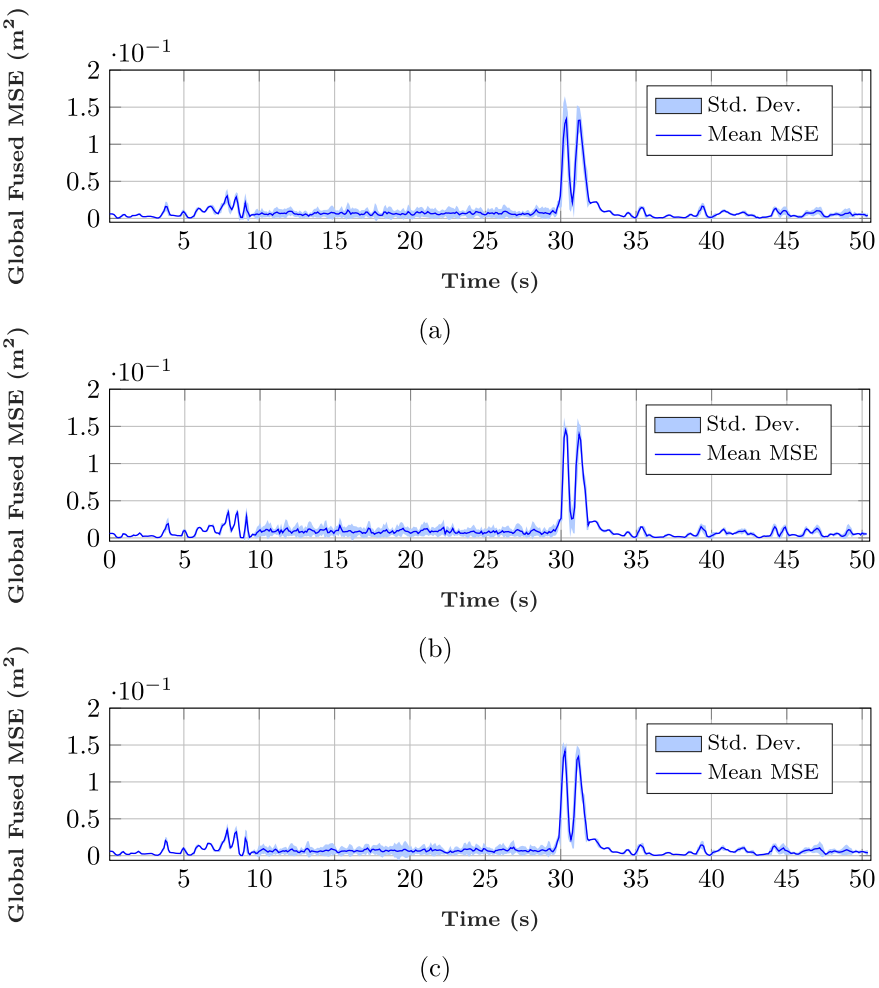

Fig. 8 Monte Carlo simulation results for path O under different noise levels. (a) $\mathcal{N}(0, 0.3^2)$, (b) $\mathcal{N}(0, 0.5^2)$, and (c) $\mathcal{N}(0, 0.7^2)$, showing the variation in global-fused Mean Squared Error (MSE) over time, with mean MSE and standard deviation

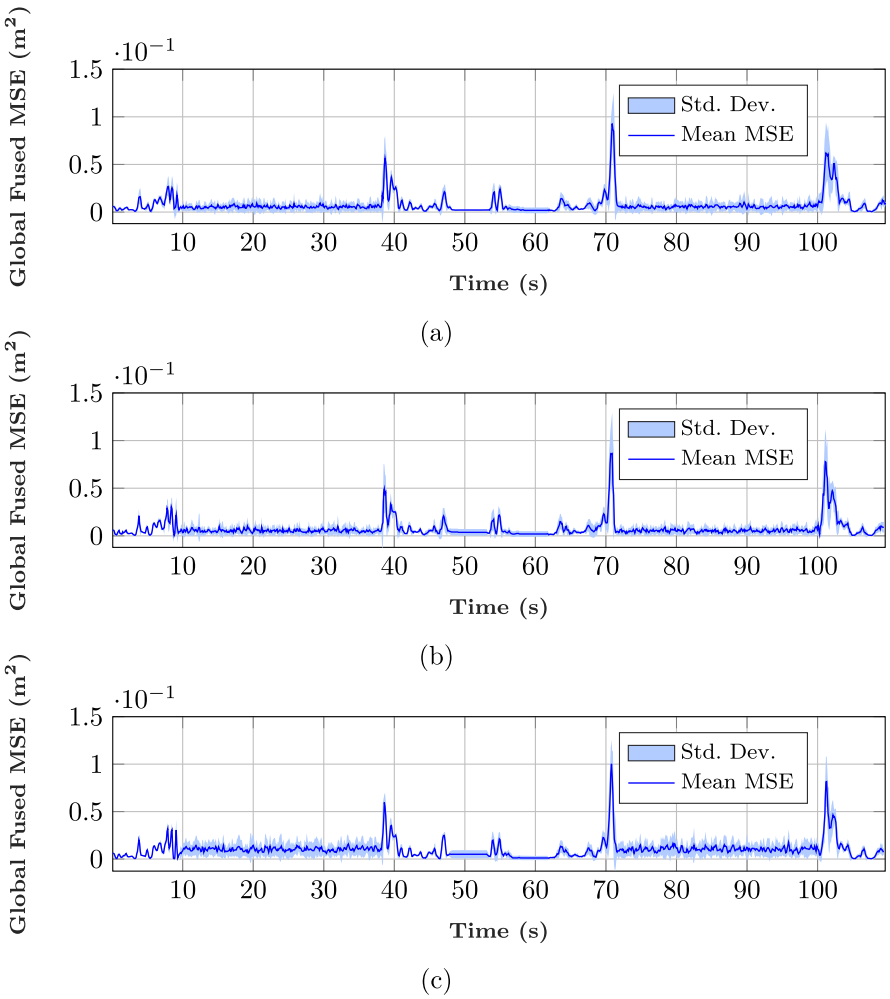

Fig. 9 Monte Carlo simulation results for path S under different noise levels. (a) $\mathcal{N}(0, 0.3^2)$, (b) $\mathcal{N}(0, 0.5^2)$, and (c) $\mathcal{N}(0, 0.7^2)$, showing the variation in global-fused MSE over time, with mean MSE and standard deviation

by summing the squares of each directional RMSE:

$$\text{MSE} = \text{RMSE}_{east}^2 + \text{RMSE}_{north}^2 = 0.339^2 + 0.291^2 \approx 0.200\, m^2 \quad (19)$$

Similarly, [29] provided their positioning accuracy in terms of Distance Root Mean Square (DRMS), with a reported value of approximately 0.0525 m. We converted DRMS to the equivalent MSE by squaring the DRMS value:

$$\text{MSE} = (\text{DRMS})^2 = 0.0525^2 \approx 0.00276\, m^2 \quad (20)$$

In comparison, our loosely-coupled integration method achieves comparable performance, with an MSE in the order of 0.01 m^2. Although direct numerical comparisons must be cautiously interpreted due to differences in sensors, experimental conditions, and integration methods, our approach clearly demonstrates competitive performance along with significant practical advantages, including reduced implementation complexity, lower computational load, and greater flexibility in sensor selection and maintenance.

5 Conclusions

This paper fundamentally addresses the challenge of maintaining seamless localization across diverse IO environments by proposing a hierarchical, loosely coupled EKF framework. Unlike purely single-sensor or tightly coupled

Table 4 Overall mean and standard deviation (Std) of MSE for paths O and S under different noise levels

Noise Level	0.3		0.5		0.7	
Path	Mean MSE	Std MSE	Mean MSE	Std MSE	Mean MSE	Std MSE
O	0.009445	0.004923	0.009565	0.004935	0.010315	0.004756
S	0.007318	0.005232	0.007436	0.005103	0.009989	0.006449

solutions, our method dynamically fuses UWB, GPS, odometry, and IMU measurements based on real-time signal quality, thereby offering robust, efficient, and adaptive localization. Through simulated scenarios, including transitions between IO areas, we have demonstrated that this hybrid approach consistently outperforms individual sensor sources by maintaining lower MSE under varying noise levels.

Beyond achieving high localization accuracy, the proposed system also finds a favorable balance between computational complexity and robustness, making it particularly suitable for resource-constrained applications such as low-cost mobile robots. However, several limitations warrant further study. First, the framework relies on pre-defined noise models; in real-world deployments, sensor noise characteristics may deviate considerably from simulated assumptions, leading to potential performance degradation. Second, the system has not yet undergone extensive real-world testing, so it remains to be seen how factors like multipath effects, dynamic crowds, or unpredictable environmental conditions might impact the final localization results. Finally, the EKF operation strongly depends on sensor-supplied covariance information, which, if inaccurately tuned, could hinder performance—especially in dynamic handover regions or high-noise scenarios.

Looking ahead, a key research direction is the dynamic estimation and refinement of sensor covariance matrices through techniques such as reinforcement learning or statistical modeling. This would enable adaptive noise adjustments and reduce reliance on pre-defined distributions. Additionally, integrating alternative localization technologies, such as LiDAR in feature-rich environments or vision-based methods in texture-dense scenes, could address situations where GPS or UWB signals are unavailable or heavily degraded. Another potential direction involves developing hybrid coupling frameworks that combine the advantages of both loose and tight coupling, alongside data-driven weighting mechanisms based on real-time quality metrics. Finally, comprehensive real-world validation in highly dynamic or cluttered spaces—like crowded urban centers, uneven terrains, and industrial warehouses—would help identify practical challenges and guide future refinements. These efforts would help enhance the reliability, scalability, and adaptability of autonomous robots navigating diverse IO environments.

Appendix A Extended Kalman Filter Principles

This appendix provides the EKF fundamentals used in our seamless indoor-outdoor localization framework and explains how each component corresponds to our application. The EKF is a recursive state estimation algorithm for nonlinear systems, which linearizes the nonlinear state and measurement models around the current estimate to apply the standard Kalman filter equations.

State Estimation Model

The system state vector $\mathbf{x}_k \in \mathbb{R}^n$ evolves according to the nonlinear discrete-time dynamic model as follows:

$$\mathbf{x}_{k+1} = \mathbf{f}(\mathbf{x}_k) + \boldsymbol{\eta}_k, \tag{A1}$$

where $\mathbf{f} : \mathbb{R}^n \times \mathbb{R}^l \to \mathbb{R}^n$ is the state transition function, and $\boldsymbol{\eta}_k \in \mathbb{R}^n$ is the process noise, assumed to be Gaussian with zero mean and covariance $\mathbf{Q}_k \in \mathbb{R}^{n\times n}$. In our system, $\mathbf{x}_k$ typically includes

$$\mathbf{x}_k = \left[x,\ y,\ z,\ \dot{x},\ \dot{y},\ \dot{z},\ \phi,\ \theta,\ \psi\right]^\top. \tag{A2}$$

representing the robot's position (x, y, z), velocity $(\dot{x}, \dot{y}, \dot{z})$, and orientation (ϕ, θ, ψ). Depending on the application requirements, certain state components can be omitted (e.g., for planar motion only).

Measurement Model

The measurement vector $\mathbf{z}_k \in \mathbb{R}^m$ is related to the state through the nonlinear measurement model as follows:

$$\mathbf{z}_k = \mathbf{h}(\mathbf{x}_k) + \boldsymbol{\nu}_k, \tag{A3}$$

where $\mathbf{h} : \mathbb{R}^n \to \mathbb{R}^m$ maps the state space to the measurement space, and $\boldsymbol{\nu}_k \in \mathbb{R}^m$ is the measurement noise, assumed to be zero-mean Gaussian with covariance $\mathbf{R}_k \in \mathbb{R}^{m\times m}$. In our case, $\mathbf{h}(\mathbf{x}_k)$ typically includes absolute position observations from GPS or UWB, as well as relative observations from the odometry and IMU. Noise covariances ($\mathbf{R}_k$) may dynamically change based on satellite geometry, multipath severity, and other environmental factors.

EKF Algorithm

The EKF algorithm consists of a prediction step and an update step.

Prediction Step

The predicted state estimate $\hat{\mathbf{x}}_{k|k-1} \in \mathbb{R}^n$ and predicted estimate covariance $\mathbf{P}_{k|k-1} \in \mathbb{R}^{n\times n}$ are computed as:

$$\hat{\mathbf{x}}_{k|k-1} = \mathbf{f}(\hat{\mathbf{x}}_{k-1|k-1}), \tag{A4}$$

$$\mathbf{P}_{k|k-1} = \mathbf{F}_{k-1}\mathbf{P}_{k-1|k-1}\mathbf{F}_{k-1}^\top + \mathbf{Q}_{k-1}, \tag{A5}$$

where $\mathbf{F}_{k-1} \in \mathbb{R}^{n\times n}$ is the Jacobian of the state transition function $\mathbf{f}$ with respect to $\mathbf{x}$, evaluated at $\hat{\mathbf{x}}_{k-1|k-1}$:

$$\mathbf{F}_{k-1} = \left.\frac{\partial \mathbf{f}}{\partial \mathbf{x}}\right|_{\hat{\mathbf{x}}_{k-1|k-1}}. \tag{A6}$$

Update Step

The Kalman gain $\mathbf{K}_k \in \mathbb{R}^{n\times m}$, updated state estimate $\hat{\mathbf{x}}_{k|k} \in \mathbb{R}^n$, and updated estimate covariance $\mathbf{P}_{k|k} \in \mathbb{R}^{n\times n}$ are computed as:

$$\mathbf{K}_k = \mathbf{P}_{k|k-1}\mathbf{H}_k^\top \left(\mathbf{H}_k\mathbf{P}_{k|k-1}\mathbf{H}_k^\top + \mathbf{R}_k\right)^{-1}, \tag{A7}$$

$$\hat{\mathbf{x}}_{k|k} = \hat{\mathbf{x}}_{k|k-1} + \mathbf{K}_k\left(\mathbf{z}_k - \mathbf{h}(\hat{\mathbf{x}}_{k|k-1})\right), \tag{A8}$$

$$\mathbf{P}_{k|k} = (\mathbf{I}_n - \mathbf{K}_k\mathbf{H}_k)\mathbf{P}_{k|k-1}, \tag{A9}$$

where $\mathbf{H}_k \in \mathbb{R}^{m\times n}$ is the Jacobian of the measurement function $\mathbf{h}$ with respect to $\mathbf{x}$, evaluated at $\hat{\mathbf{x}}_{k|k-1}$:

$$\mathbf{H}_k = \left.\frac{\partial \mathbf{h}}{\partial \mathbf{x}}\right|_{\hat{\mathbf{x}}_{k|k-1}}, \tag{A10}$$

and $\mathbf{I}_n$ is the $n \times n$ identity matrix.

Additional Explanations of the Matrices

- $\mathbf{F}_{k-1}$ (State Transition Jacobian): This matrix is derived by linearizing the robot's motion model (i.e., $\mathbf{f}_L$) with respect to the state vector. It quantifies how small changes in the state affect the predicted state, reflecting the sensitivity of the motion dynamics.
- $\mathbf{P}_{k|k-1}$ and $\mathbf{P}_{k|k}$ (State Covariance Matrices): These matrices represent the uncertainty in the state estimates before and after the measurement update, respectively. They capture the effects of process noise and measurement noise in our system.
- $\mathbf{K}_k$ (Kalman Gain): Specifies how much weight the sensor measurements (e.g., odometry and IMU data) carry in correcting the predicted state. A larger Kalman gain indicates higher confidence in measurement data for that update.
- $\mathbf{H}_k$ (Measurement Jacobian): This matrix is obtained by linearizing the measurement function $\mathbf{h}_L$ with respect to the state vector. It maps the uncertainties in the state space to the measurement space, reflecting how sensitive the sensor outputs (such as acceleration and angular velocities) are to changes in the state.
- $\mathbf{I}_n$ (Identity Matrix): The identity matrix that ensures dimensionally correct covariance updates.

Acknowledgements This work was carried out within the MOST - Sustainable Mobility National Research Center and received funding from the European Union Next-GenerationEU (PIANO NAZIONALE DI RIPRESA E RESILIENZA (PNRR) - MISSIONE 4 COMPONENTE 2, INVESTIMENTO 1.4 - D.D. 1033 17/06/2022, CN00000023). This manuscript reflects only the authors' views and opinions, neither the European Union nor the European Commission can be considered responsible for them.

Author Contributions Y. Cao (Conceptualization, Methodology, Algorithm Development, Literature Review, Simulation Software Implementation, Data Curation, Results Analysis, and Manuscript Draft Preparation); A. Usai (Data Curation, Structural Improvements, Content Optimization, Language Edits, Manuscript Revision); W. Gu (Manuscript Review and Project Guidance); A. Rizzo (Research Coordination, Supervision, and Manuscript Revision).

Data Availability Data sets generated during the current study are available from the corresponding author on reasonable request.

Declarations

Competing Interests Alessandro Rizzo is a Senior Editor at Large of the Journal of Intelligent and Robotic Systems. The authors declare no additional conflicts of interest.

Ethics Approval and Consent to Participate Not applicable.

Consent for Publication Not applicable.

References

1. Chen, S., Feng, T., Luo, X., Li, J., Luo, Y., Teng, Y., et al.: Research on high-precision localization method for transport robots in industrial environments based on Improved AMCL and QR code assistance. Sci. Reports. **02**, 15 (2025). https://doi.org/10.1038/s41598-024-85067-8
2. Zhetao Zhang, H.Y., He, X., Zeng, J.: Cycle slip detection and repair based on the unmodeled-error-constrained geometry-free combining geometry-based models for a single-frequency receiver. Measurement. **217**, 113090 (2023)
3. Maduranga, M.W.P., Tilwari, V., Abeysekera, R.: Improved-RSSI-based indoor localization by using pseudo-linear solution with machine learning algorithms. J. Electrical Syst. Inf. Technol. **11**, 10 (2024). https://doi.org/10.1186/s43067-024-00138-0
4. Guo, H., Song, S., Yin, H., et al.: Optimization of UWB indoor positioning based on hardware accelerated Fuzzy ISODATA. Sci.

Reports. **14**, 17985 (2024). https://doi.org/10.1038/s41598-024-68998-0
5. Cadena, C., Carlone, L., Carrillo, H., Latif, Y., Scaramuzza, D., Neira, J., et al.: Past, Present, and Future of Simultaneous Localization and Mapping: Toward the Robust-Perception Age. IEEE Trans. Robot. **32**, 1309–1332 (2016)
6. Thrun, S., Burgard, W., Fox, D.: Probabilistic Robot., 1st edn. MIT Press, Cambridge, MA (2005)
7. Cadena, C., et al.: Past, Present, and Future of Simultaneous Localization and Mapping: Towards the Robust-Perception Age. IEEE Trans. Robot. (2016)
8. Mallik, M., Panja, A.K., Chowdhury, C.: Paving the way with machine learning for seamless indoor–outdoor positioning: A survey. Inf. Fusion. **94**, 126–151 (2023). https://doi.org/10.1016/j.inffus.2023.01.023
9. Zhu, Y., Luo, H., Wang, Q., Zhao, F., Ning, B., Ke, Q., et al.: A Fast Indoor/Outdoor Transition Detection Algorithm Based on Machine Learning. Sensors. **19**(4), 786 (2019). https://doi.org/10.3390/s19040786
10. Alinsavath, K.N., Nugroho, L.E., Widyawan, Hamamoto K.: The Seamlessness of Outdoor and Indoor Localization Approaches based on a Ubiquitous Computing Environment: A Survey. In: Proceedings of the 2nd International Conference on Information Science and Systems (2019)
11. Alatise, M.B., Hancke, G.P.: A Review on Challenges of Autonomous Mobile Robot and Sensor Fusion Methods. IEEE Access. **8**, 39830–39846 (2020). https://doi.org/10.1109/ACCESS.2020.2975643
12. Medeiros, R.A., Pimentel, G.A., Garibotti, R.: An Embedded Quaternion-Based Extended Kalman Filter Pose Estimation for Six Degrees of Freedom Systems. J. Intell. Robot. Syst. **102**, 18 (2021). https://doi.org/10.1007/s10846-021-01377-3
13. D'Alfonso, L., Lucia, W., Muraca, P., Pugliese, P.: Mobile robot localization via EKF and UKF: A comparison based on real data. Robot. Autonom. Syst. **07**, 74 (2015). https://doi.org/10.1016/j.robot.2015.07.007
14. Ullah, I., Shen, Y.R., Su, X., Esposito, C., Choi, C.: A Localization Based on Unscented Kalman Filter and Particle Filter Localization Algorithms. IEEE Access. **8**, 2233–2246 (2020)
15. Rigatos, G.G.: Extended Kalman and Particle Filtering for sensor fusion in motion control of mobile robots. Math. Comput. Simulat. **81**(3), 590–607 (2010). https://doi.org/10.1016/j.matcom.2010.05.003
16. Cherif, M.L., Leclère, J., Landry, R.J., Loosely coupled GPS, INS integration with snap to road for low-cost land vehicle navigation: EKF-STR for low-cost applications. In,: IEEE/ION Position. Location Navigation Symposium (PLANS) **2018**, 275–282 (2018)
17. Anjum, M.L., Park, J., Hwang, W., Kwon, H.i., Kim, J.h., Lee, C., et al.: Sensor data fusion using Unscented Kalman Filter for accurate localization of mobile robots. In: ICCAS **2010**, 947–952 (2010)
18. Ren, Y., Ke, X.: Particle Filter Data Fusion Enhancements for MEMS-IMU/GPS. Intell. Inf. Manag. **2**(7), 417–421 (2010). https://doi.org/10.4236/iim.2010.27051
19. Cappello, F., Sabatini, R., Ramasamy, S., Marino, M.: Particle filter based multi-sensor data fusion techniques for RPAS navigation and guidance. In: 2015 IEEE Metrology for Aerospace (MetroAeroSpace). pp. 395–400 (2015)
20. He, C., Tang, C., Yu, C.: A Federated Derivative Cubature Kalman Filter for IMU-UWB Indoor Positioning. Sensors. **20**, 3514 (2020). https://doi.org/10.3390/s20123514
21. Li, N., Guan, L., Gao, Y., Du, S., Wu, M., Guang, X., et al.: Indoor and Outdoor Low-Cost Seamless Integrated Navigation System Based on the Integration of INS/GNSS/LIDAR System. Remote Sens. **12**, 3271 (2020). https://doi.org/10.3390/rs12193271
22. Cheng, J., Yang, L., Li, Y., Zhang, W.: Seamless outdoor/indoor navigation with WIFI/GPS aided low cost Inertial Navigation System. Phys. Commun. **13**(Part A), 31–43 (2014). https://doi.org/10.1016/j.phycom.2013.12.003
23. Jiang, W., Li, Y., Rizos, C., Cai, B., Shangguan, W.: Seamless Indoor-Outdoor Navigation based on GNSS, INS and Terrestrial Ranging Techniques. J. Navigation. **70**(6), 1183–1204 (2017). https://doi.org/10.1017/S037346331700042X
24. Zhu, N., Ortiz, M., Renaudin, V.: Seamless Indoor-Outdoor Infrastructure-free Navigation for Pedestrians and Vehicles with GNSS-aided Foot-mounted IMU. In: 2019 International Conference on Indoor Positioning and Indoor Navigation (IPIN); pp. 1–8 (2019)
25. Yin, H., Xu, X., Lu, S., et al.: A Survey on Global LiDAR Localization: Challenges, Advances and Open Problems. Int. J. Comput. Vision. **132**, 3139–3171 (2024). https://doi.org/10.1007/s11263-024-02019-5
26. He, S., Chan, S.H.G.: Wi-Fi Fingerprint-Based Indoor Positioning: Recent Advances and Comparisons. IEEE Commun. Surv. Tutorials. **18**(1), 466–490 (2016). https://doi.org/10.1109/COMST.2015.2464084
27. Wang, J., Gao, Y., Liu, Z.: Pseudolite Applications in Positioning and Navigation: Progress and Problems. J. Navigation. **71**(1), 1–20 (2018)
28. Villien, C., Denis, B., UWB-aided GNSS, INS Fusion for Resilient Positioning in GNSS Challenged Environments. In,: IEEE/ION Position. Location Navigation Symposium (PLANS) **2023**, 167–178 (2023)
29. Jiang, W., Cao, Z., Cai, B., Li, B., Wang, J.: Indoor and Outdoor Seamless Positioning Method Using UWB Enhanced Multi-Sensor Tightly-Coupled Integration. IEEE Trans. Vehic. Technol. **70**(10), 10633–10645 (2021). https://doi.org/10.1109/TVT.2021.3110325
30. Li, X., Wu, Z., Shen, Z., Xu, Z., Li, X., Li, S., et al.: An Indoor and Outdoor Seamless Positioning System for Low-Cost UGV Using PPP/INS/UWB Tightly Coupled Integration. IEEE Sensors J. **23**(20), 24895–24906 (2023). https://doi.org/10.1109/JSEN.2023.3310480
31. Zhang, K., Shen, C., Zhou, Q., Wang, H., Gao, Q., Chen, Y.: A combined GPS UWB and MARG locationing algorithm for indoor and outdoor mixed scenario. Cluster Comput. **22**, 5965–5974 (2019)
32. Luo, J., Yin, Z., Gui, L., Yang, X.: Accurate Localization for Indoor and Outdoor Scenario by GPS and UWB Fusion. In: 2023 9th International Conference on Control, Automation and Robotics (ICCAR); pp. 411–416 (2023)
33. Agarwal, S., Mierle, K., Others.: Ceres Solver. Accessed: 2024-11-22. Available from: http://ceres-solver.org
34. Zeng, Q., Wang, J., Meng, Q., Zhang, X., Zeng, S.: Seamless Pedestrian Navigation Methodology Optimized for Indoor/Outdoor Detection. IEEE Sensors J. **18**(1), 363–374 (2018). https://doi.org/10.1109/JSEN.2017.2764509
35. Hansen, R., Wind, R., Jensen, C.S., Thomsen, B.: Seamless Indoor/Outdoor Positioning Handover for Location-Based Services in Streamspin. In: 2009 Tenth International Conference on Mobile Data Management: Systems, Services and Middleware; pp. 267–272 (2009)
36. Zou, D., liang Deng, Z., Xu, L., Ren, W.: Seamless LBS Based on the Integration of WSN and GPS. In: 2008 International Symposium on Computer Science and Computational Technology. **2**, 91–96 (2008)
37. Liu, X., Man, Q., Lu, H., Lin, X.: Wi-Fi/MARG/GPS integrated system for seamless mobile positioning. In: 2013 IEEE Wireless Communications and Networking Conference (WCNC) pp. 2323–2328 (2013)
38. Jia, M., Yang, Y., Kuang, L., Xu, W., Chu, T., Song, H.: An Indoor and Outdoor Seamless Positioning System Based on Android Plat-

form. In: 2016 IEEE Trustcom/BigDataSE/ISPA. pp. 1114–1120 (2016)
39. Wen, W., Bai, X., Kan, Y.C., Hsu, L.T.: Tightly Coupled GNSS/INS Integration via Factor Graph and Aided by Fish-Eye Camera. IEEE Trans. Vehic. Technol. **68**(11), 10651–10662 (2019). https://doi.org/10.1109/TVT.2019.2944680
40. Zhang, J., Khoshelham, K., Khodabandeh, A.: Seamless vehicle positioning by lidar-GNSS integration: standalone and multi-epoch scenarios. Remote Sens. **13**(22), 4525 (2021)
41. Yao, L., Li, M., Xu, T., Dai, X., Jiang, T., Dai, P., et al.: GNSS/UWB/INS indoor and outdoor seamless positioning algorithm based on federal filtering. Measurement Sci. Technol. **35**, 015135 (2023)
42. Odenes, J., Enefjord, T.: robot_localization: Extended Kalman Filter and Unscented Kalman Filter for State Estimation in ROS. In: Proceedings of the 2015 International Conference on Robotics and Automation (ICRA). IEEE, pp. 2624–2631 (2015)
43. Open Robotics.: ROS 2 Humble Documentation. Available from: https://docs.ros.org/en/humble/index.html
44. Open Robotics.: Gazebo Simulator. Available from: http://gazebosim.org/
45. Robotis.: TurtleBot3. Available from: https://emanual.robotis.com/docs/en/platform/turtlebot3/overview/
46. Moore, T., Stouch, D.W.: A Generalized Extended Kalman Filter Implementation for the Robot Operating System. In: Annual Meeting of the IEEE Industry Applications Society (2014). Available from: https://api.semanticscholar.org/CorpusID:26564553
47. Huang, Y., Cao, B., Wang, A.: Design a novel algorithm for enhancing UWB positioning accuracy in GPS denied environments. Sci. Reports. **14**, 23895 (2024). https://doi.org/10.1038/s41598-024-74773-y

Yuan Cao is currently pursuing a Ph.D. in Electronics and Telecommunications at Politecnico di Torino, Italy. He received his B.Sc. in Mechanical Engineering in 2020 and his M.Sc. in Mechatronic Engineering in 2022 from the same institution. His research interests are centered on adaptive and learning-based control methods, including backstepping techniques and sensor fusion, for UAVs and mobile robots.

Andrea Usai (Graduate Student Member, IEEE) received the B.Sc. degree in mechanical engineering and the M.Sc. degree in mechatronics engineering from the Politecnico di Torino, Italy, in 2021 and 2023, respectively, where he is currently pursuing the Ph.D. degree in electrical, electronics and communications engineering. His research interests include robotics, neuro-inspired control architectures, and machine learning, with a focus on nonlinear systems and applications to UAVs and mobile robots.

Weibin Gu is currently a Postdoctoral Researcher at the Institute for AI Industry Research (AIR), Tsinghua University, China. He earned his Ph.D. in Electronics and Telecommunications from Politecnico di Torino, Italy, in 2024, his M.Sc. in Mechatronic Engineering from the same institution in 2017, and his B.Sc. in Mechanical Engineering through a dual-degree program at Tongji University, China, and Politecnico di Torino in 2015. From September 2019 to October 2020, he served as a Flight Control Engineer and Project Lead at Shanghai FOIA Co., Ltd., China, where he led a UAV-based autonomous project for industrial applications. Between 2017 and 2020, he also collaborated on UAV research with the University of Denver, U.S., and Politecnico di Torino. His research interests are centered on the intersection of machine learning and control theory, with a focus on real-world robotic and autonomous systems.

Alessandro Rizzo is an Associate Professor at the Department of Electronics and Telecommunications, Politecnico di Torino, Italy, where he coordinates the Complex Systems Laboratory. He received his Laurea degree in Computer Engineering, summa cum laude, and his PhD in Automation and Electronics Engineering from the University of Catania, Italy, in 1996 and 2000, respectively. Dr. Rizzo's previous affiliations include JET Joint Undertaking (UK), ST Microelectronics (Italy), the University of Messina (Italy), Politecnico di Bari (Italy), and New York University (USA). His research interests span complex networks and systems, robotics, and modeling and control of nonlinear systems. He has authored two books, holds two international patents, and has published over 200 papers in peer-reviewed international journals and conference proceedings. A Distinguished Lecturer for the IEEE Nuclear and Plasma Sciences Society, he received the Best Application Paper Award at the 2002 IFAC World Congress, as well as two Amazon Research Awards in Robotics (2019 and 2021).